Title : Hardware-in-the-Loop Simulation of Vehicle-Manipulator Systems for Physical Interaction tasks

Authors : Hemjyoti Das, Bjørn Kare Sæbø, Kristin Y. Pettersen and Christian Ott

Hardware-in-the-Loop Simulation of Vehicle-Manipulator Systems for Physical Interaction Tasks

Hemjyoti Das[1], Bjørn Kåre Sæbø[2], Kristin Y. Pettersen[2] and Christian Ott[1,3]

Abstract— Hardware-in-the-loop simulation (HILS) allows a more realistic evaluation of control approaches than what is possible with pure software simulations, but without the actual complexity of the complete system. This is important for some complex systems such as orbital robots, where testing of the system is typically not possible after its launch, and an on-ground replica is used to validate the performance of such a system. In this article, an impedance-matching approach is presented to match the end-effector dynamics of a fixed-base robot manipulator with that of a target vehicle-manipulator system (VMS), while taking into account the redundant nullspace dynamics in a connected real-time simulation framework. This approach ensures that the forces and torques exerted by the system on the environment matches with that of the simulated system. The contact wrenches used in our approach are not obtained from numerical simulations, but rather from real physical interaction, which is one of the main advantages of our approach. The effectiveness of our method is validated by demonstrating various physical interaction tasks with the environment, using a suspended aerial manipulator as the target system.

I. INTRODUCTION

Vehicle-manipulator systems (VMS) combine the benefits of traditional fixed-base manipulators (FBM), with the versatility of a mobile base. In some applications such as orbital [1], or underwater [2] robotics, a mobile base is required to reach the working area. Mobile robots often work in environments that are hazardous or unreachable by humans, besides their widespread use in common industrial and household automation tasks where it is not constrained to a fixed location. Examples include space robotics [3] and underwater intervention [4].

In many cases, full scale tests of the VMS are prohibitively expensive or practically impossible to perform before the system is put into use. Computer simulations allow initial tests of software and controller design, but are limited in

[1]The authors are with the Automation and Control Institute (ACIN), Faculty of Electrical Engineering and Information Technology, Technical University of Vienna, TU Wien, Gusshausstraße 27-29, A-1040, Vienna, Austria {hemjyoti.das, christian.ott}@tuwien.ac.at

[2]The authors are with the Centre for Autonomous Marine Operations and Systems (NTNU AMOS), Department of Engineering Cybernetics, Norwegian University of Science and Technology, NTNU, NO-7491 Trondheim, Norway {bjorn.k.sabo, kristin.y.pettersen}@ntnu.no

[3] The author is with the Institute of Robotics and Mechatronics, German Aerospace Center (DLR), Oberpfaffenhofen, Muenchener Strasse 20, 82234, Wessling, Germany

several ways. Such simulations usually are based on simplified models of the system and the environment, which can possibly omit some important information such as the contact dynamics that are hard to model accurately [5]. Additionally, completely numerical simulations do not allow the testing of the components used during the actual experiments. It is therefore common to use hardware-in-the-loop simulations (HILS), where physical components of the actual system are integrated into the simulation [6], [7].

HILS has been widely used for several decades, with early works on flight and missile simulations [6], [8], as well as in the automotive industry [9]. Testing of robotic systems for use in space is often done using HILS in on-ground testing facilities [10]–[12]. Typically, these facilities use a fixed-base manipulator arm to emulate an on-orbit manipulator arm, and a second arm to emulate the environment or a manipulator base. One exception is [1], in which a HILS method is developed, using a fixed-base robot to emulate the joint dynamics of a VMS in orbit. This approach uses external forces in the simulation, but cannot interact with the real environment. In [13], HILS of a space manipulator arm is accomplished by enforcing a forward kinematics from the simulation onto an industrial robot, while obtaining its sensory feedback and transmitting it back to the simulation. Even though these methods allows physical interaction, it is formulated at the kinematic level and is validated with a single degree of freedom (DoF) robot.

In [14], an underwater vehicle–manipulator system (UVMS) is emulated by mounting a KUKA IIWA14 robotic manipulator on a Stewart Platform in order to perform physical interactions with the environment. In [15], a method is developed that allows a ground robot to emulate the end-effector dynamics of an orbital manipulator during interaction tasks. A constraint dynamics formulation is used in their work, whereas our formulation relies on classical impedance control. The proposed solution in [15] does not allow the use of a redundant fixed-base manipulator as it relies on the inverse of the manipulator Jacobian, which is addressed in our work. Additionally, their proposed solution for a redundant VMS utilizes a kinematic nullspace that is inertially coupled and thus depends on the measured external force. In contrast, our work uses a dynamically consistent nullspace projection, which is independent of the measured external forces. The evaluation of the work in [15] is done only on a 1-DoF system, whereas our work is validated on a completely redundant 7-DoF arm.

In [16], HILS has been demonstrated for performing physical human-aerial manipulator cooperation, which ad-

dresses a similar application as our paper. However, their work relies on a computer simulation of the VMS based on measured forces. An user can interact with the simulated VMS dynamics by means of a haptic display, which is controlled in an admittance mode. Instead, we apply an impedance control approach which is used to implement the end-effector dynamics of the VMS directly onto the FBM. In this way, the FBM displays the correct inertial behavior of the VMS.

This article focuses on utilizing an off-the-shelf FBM to emulate a VMS, matching the end-effector dynamics and interaction forces with the simulated system. The main contributions of this paper can be summarized as the development of a hardware-in-the-loop simulation framework for VMS, based on an impedance-matching framework, that allows interaction with the environment by considering the contact forces. Additionally, redundancy involved with the extra-degrees of freedom is handled by using inertially-decoupled nullspace dynamics, which are simulated in a closed loop with the end-effector dynamics. Our algorithm is generic as it can be applied to match the end-effector dynamics of a given VMS, regardless of its structure and the total DoFs. The proposed framework is validated experimentally by mapping the end-effector dynamics of a 10-DoF suspended aerial manipulator system with that of a 7-DoF Franka Research 3 robot manipulator [17], while successfully demonstrating various physical interaction tasks. The generic nature of our algorithm is demonstrated by considering two different configurations of the VMS.

The paper is organized as follows. In Sec. II, some mathematical background and the dynamical models of the systems are presented. In Sec. III, the proposed method of impedance matching is developed, while the implemented controller is discussed in Sec. IV. The results from the experimental validation are presented in Sec. V. Finally, the conclusions and ideas for future work are given in Sec. VI.

II. END-EFFECTOR DYNAMICS OF THE MANIPULATOR SYSTEMS

In this section, mathematical models of a general FBM and a VMS are presented. Since our approach relies on mapping the end-effector dynamics of the VMS onto that of the FBM, both the models are transformed into Cartesian end-effector coordinates. Mapping of the end-effector dynamics will ensure that real contact forces experienced by the FBM will influence the dynamics of the VMS, and thus allows us to accomplish HILS-based physical interaction with the environment. While the end-effector dynamics of the VMS is aimed to be emulated by the FBM, the remaining degrees of freedom of the VMS must be simulated numerically. Due to the associated noise of acceleration measurements, utilizing them directly in the numeric simulation may severely impact its performance [1]. Therefore, nullspace coordinates [18] are utilized to express the complete system dynamics in an inertially decoupled form, where the nullspace dynamics does not impact the end-effector's acceleration. Moreover, in contrast to [19], the nullspace dynamics are unaffected by

the contact forces at the end-effector, which is an additional benefit of our approach.

A. Fixed-base Manipulator

The configuration of a fixed-base manipulator (FBM) consists of n revolute or prismatic joints, whose states are described by the vector $\boldsymbol{q} \in \mathbb{R}^n$. The dynamics of the system are given as,

$$\boldsymbol{M}(\boldsymbol{q})\ddot{\boldsymbol{q}} + \boldsymbol{C}(\boldsymbol{q},\dot{\boldsymbol{q}})\dot{\boldsymbol{q}} + \boldsymbol{g}(\boldsymbol{q}) = \boldsymbol{\tau} + \boldsymbol{J}_e^T(\boldsymbol{q})\boldsymbol{F}_{\text{ext}}, \quad (1)$$

where $\boldsymbol{M}(\boldsymbol{q}) \in \mathbb{R}^{n \times n}$ is the inertia matrix in the joint space, $\boldsymbol{C}(\boldsymbol{q},\dot{\boldsymbol{q}})\dot{\boldsymbol{q}} \in \mathbb{R}^n$ consists of the Coriolis and centrifugal terms, and $\boldsymbol{g}(\boldsymbol{q}) \in \mathbb{R}^n$ is the gravitational force acting on the joints. The commanded joint torques are denoted as $\boldsymbol{\tau} \in \mathbb{R}^n$ and the external wrench applied at the end-effector as $\boldsymbol{F}_{\text{ext}} \in \mathbb{R}^6$, while the end-effector Jacobian is denoted as $\boldsymbol{J}_e \in \mathbb{R}^{6 \times n}$ [20]. From this point on, for notational clarity, dependencies of the terms will be omitted. The pose of the end-effector is denoted as $\boldsymbol{x}_e \in \mathbb{R}^6$, consisting of position and orientation, and its velocity is related to the joint velocities as,

$$\dot{\boldsymbol{x}}_e = \boldsymbol{J}_e \dot{\boldsymbol{q}}. \quad (2)$$

The joint space of the FBM may have a higher dimension than the states of the end-effector, (which in our case is 6). Therefore, by considering that the joint space has a dimension $n > 6$, a redundancy is involved that is accounted for by defining the nullspace velocity $\boldsymbol{v_n} \in \mathbb{R}^{n-6}$, which is related to the joint space using the nullspace Jacobian $\boldsymbol{N}(\boldsymbol{q})$ as follows,

$$\boldsymbol{v_n} = \boldsymbol{N}(\boldsymbol{q})\dot{\boldsymbol{q}}. \quad (3)$$

The nullspace Jacobian matrix $\boldsymbol{N}(\boldsymbol{q})$ is based on [18] and is chosen as follows,

$$\boldsymbol{N}(\boldsymbol{q}) = \left(\boldsymbol{Z}(\boldsymbol{q})\boldsymbol{M}(\boldsymbol{q})\boldsymbol{Z}(\boldsymbol{q})^T\right)^{-1}\boldsymbol{Z}(\boldsymbol{q})\boldsymbol{M}(\boldsymbol{q}), \quad (4)$$

where the nullspace base matrix $\boldsymbol{Z}$ can be chosen using different techniques [21] to satisfy

$$\boldsymbol{J}_e(\boldsymbol{q})\boldsymbol{Z}(\boldsymbol{q})^T = \boldsymbol{0}. \quad (5)$$

Eq. (4) ensures an inertial decoupling between the end-effector and nullspace dynamics [18]. The nullspace velocities $\boldsymbol{v_n}$ and their integrals do not correspond to a physical quantity of the system, but are rather used to describe the redundant motion of the system. Combining the end-effector and the nullspace velocity, the new velocity vector $\dot{\boldsymbol{x}}$ and augmented Jacobian $\boldsymbol{J}$ of the FBM are expressed as follows,

$$\dot{\boldsymbol{x}} = \begin{bmatrix} \dot{\boldsymbol{x}}_e \\ \boldsymbol{v_n} \end{bmatrix} = \begin{bmatrix} \boldsymbol{J}_e \\ \boldsymbol{N} \end{bmatrix} \dot{\boldsymbol{q}} = \boldsymbol{J}\dot{\boldsymbol{q}}. \quad (6)$$

We consider that the commanded torque $\boldsymbol{\tau}$ compensates for the effect of gravity, leading us to the effective commanded torque $\boldsymbol{\tau} = \boldsymbol{\tau}' + \boldsymbol{g}$. To analyze the effect of the control torque in the end-effector and nullspace coordinates, we can define the torque $\boldsymbol{\tau}'$ as a function of a desired end-effector control force $\boldsymbol{F}_e$ and nullspace control force $\boldsymbol{F}_n$. Specifically, we can express $\boldsymbol{\tau}' = \boldsymbol{J}_e^T \boldsymbol{F}_e + \boldsymbol{N}^T \boldsymbol{F}_n$ and $\boldsymbol{F} = \begin{bmatrix} \boldsymbol{F}_e^T & \boldsymbol{F}_n^T \end{bmatrix}^T$. The design of the control forces is done

in Sec. IV. Next, differentiating (6) and utilizing (1), the end-effector and nullspace dynamics are found as follows,

$$\ddot{x} = JM^{-1}J^T F + JM^{-1}J_e^T F_{\text{ext}} - JM^{-1}C\dot{q} + \dot{J}\dot{q}. \quad (7)$$

A task inertia matrix is defined as $\Lambda = (JM^{-1}J^T)^{-1}$, and a task Coriolis matrix as $\mu = \Lambda JM^{-1}CJ^{-1} - \Lambda \dot{J}J^{-1}$. Utilizing these definitions, Eq. (7) is reformulated as follows,

$$\underbrace{\begin{bmatrix} \Lambda_e & 0 \\ 0 & \Lambda_n \end{bmatrix}}_{\Lambda} \begin{bmatrix} \ddot{x}_e \\ \dot{v}_n \end{bmatrix} + \underbrace{\begin{bmatrix} \mu_e & \mu_{en} \\ \mu_{ne} & \mu_n \end{bmatrix}}_{\mu} \begin{bmatrix} \dot{x}_e \\ v_n \end{bmatrix} = \begin{bmatrix} F_e + F_{\text{ext}} \\ F_n \end{bmatrix}. \quad (8)$$

The block diagonal structure of Λ, and the fact that the task forces only affect the end-effector coordinates, are because of the particular choice of the dynamically consistent nullspace Jacobian N. Additionally, the external force at the end-effector, F_{ext}, does not affect the nullspace dynamics. Note that there is still a coupling between the coordinates at the velocity level due to the Coriolis matrix μ.

B. Vehicle-Manipulator System

We consider a VMS consisting of a mobile base with a manipulator arm attached to it. Throughout the paper, quantities with a hat operator $(\hat{\cdot})$ refer to the VMS. The system state can be described by a vector $\hat{\eta} \in \mathbb{R}^{\hat{m}+\hat{n}}$, where $\hat{m}$ is the number of DoFs of the system base, and $\hat{n}$ is the number of manipulator joints. For a floating base in $SE(3)$, we have $\hat{m} = 6$. A vector of quasi-velocities $\hat{\nu} \in \mathbb{R}^{\hat{m}+\hat{n}}$ is also defined, containing the base velocity vector $\hat{v}_b \in \mathbb{R}^{\hat{m}}$ and the joint velocities $\dot{\hat{q}} \in \mathbb{R}^{\hat{n}}$ such that

$$\hat{\eta} = \begin{bmatrix} \hat{x}_b^T & \hat{q}^T \end{bmatrix}^T \quad \hat{\nu} = \begin{bmatrix} \hat{v}_b^T & \dot{\hat{q}}^T \end{bmatrix}^T. \quad (9)$$

The dynamics of the system can be described as follows,

$$\hat{M}(\hat{q})\dot{\hat{\nu}} + \hat{C}(\hat{q}, \hat{\nu})\hat{\nu} + \hat{g}(\hat{\eta}) = \hat{\tau} + \hat{J}_e^T \hat{F}_{\text{ext}}. \quad (10)$$

Here it is assumed that the external forces only affect the end-effector of the system. The matrix $\hat{M} \in \mathbb{R}^{(\hat{m}+\hat{n})\times(\hat{m}+\hat{n})}$ is the inertia matrix, $\hat{C} \in \mathbb{R}^{(\hat{m}+\hat{n})\times(\hat{m}+\hat{n})}$ is the Coriolis and centrifugal matrix, and $\hat{g} \in \mathbb{R}^{(\hat{m}+\hat{n})}$ is the vector of potential forces (gravity). The control input is given by $\hat{\tau} \in \mathbb{R}^{\hat{m}+\hat{n}}$. The Jacobian matrix $\hat{J}_e \in \mathbb{R}^{6\times(\hat{m}+\hat{n})}$ is the end-effector Jacobian. Finally, $\hat{F}_{\text{ext}} \in \mathbb{R}^6$ are the external forces and torques acting at the end-effector. When $\hat{m} + \hat{n} > 6$, the system is redundant, and the end-effector coordinates are not sufficient to describe the full system state. Therefore, the nullspace velocities of the VMS are developed similarly to (4), giving the augmented Jacobian as,

$$\hat{J} = \begin{bmatrix} \hat{J}_e^T & \hat{N}^T \end{bmatrix}^T. \quad (11)$$

Next, defining the task inertia matrix $\hat{\Lambda} = (\hat{J}\hat{M}^{-1}\hat{J}^T)^{-1}$, the task Coriolis matrix $\hat{\mu} = \hat{\Lambda}\left(\hat{J}\hat{M}^{-1}\hat{C} - \dot{\hat{J}}\right)\hat{J}^{-1}$, and the task gravity vector $\hat{\rho} = \hat{\Lambda}\hat{J}\hat{M}^{-1}\hat{g}$ allows us to write the dynamics in end-effector and nullspace velocity coordinates as,

$$\begin{bmatrix} \hat{\Lambda}_e & 0 \\ 0 & \hat{\Lambda}_n \end{bmatrix} \begin{bmatrix} \ddot{\hat{x}}_e \\ \dot{\hat{v}}_n \end{bmatrix} + \begin{bmatrix} \hat{\mu}_e & \hat{\mu}_{en} \\ \hat{\mu}_{ne} & \hat{\mu}_n \end{bmatrix} \begin{bmatrix} \dot{\hat{x}}_e \\ \hat{v}_n \end{bmatrix} + \begin{bmatrix} \hat{\rho}_e \\ \hat{\rho}_n \end{bmatrix} = \begin{bmatrix} \hat{F}_e + \hat{F}_{\text{ext}} \\ \hat{F}_n \end{bmatrix}. \quad (12)$$
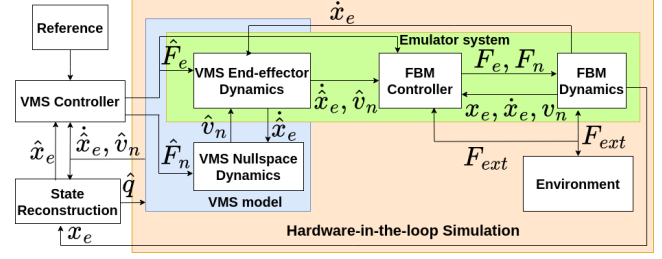

Fig. 1: Block diagram of our proposed HILS approach

III. IMPEDANCE MATCHING STRATEGY

In this section, we develop the proposed method of impedance matching, whose goal is to map the end-effector dynamics of the VMS (15) to the end-effector dynamics of the FBM (8), since a main focus of this work is to achieve realistic contact dynamics between the end-effector and the environment. To this end, the applied control force at the end-effector of the HILS-manipulator should cancel its end-effector dynamics, and insert the corresponding dynamics of the VMS. A block diagram of our proposed approach is shown in Fig. 1. The control force is chosen as

$$F_e = \Lambda_e \ddot{\hat{x}}_e + \mu_e \dot{x}_e + \mu_{en} v_n - F_{\text{ext}}, \quad (13)$$

which by (8) leads to the FBM end-effector acceleration as,

$$\ddot{x}_e = \ddot{\hat{x}}_e. \quad (14)$$

The VMS dynamics derived in (12) has the same inertially decoupled structure as the coordinates used in [22], allowing us to express the dynamics of the VMS end-effector as,

$$\ddot{\hat{x}}_e = \hat{\Lambda}_e^{-1}\left(\hat{F}_e + \hat{F}_{\text{ext}} - \hat{\rho}_e - \hat{\mu}_e \dot{\hat{x}}_e - \hat{\mu}_{en}\hat{v}_n\right), \quad (15)$$

which does not rely on the nullspace accelerations. Equivalently, the nullspace dynamics are given as,

$$\dot{\hat{v}}_n = \hat{\Lambda}_n^{-1}\left(\hat{F}_n - \hat{\rho}_n - \hat{\mu}_n \hat{v}_n - \hat{\mu}_{en}\dot{\hat{x}}_e\right). \quad (16)$$

In order to match the interaction forces, we set $\hat{F}_{\text{ext}} = F_{\text{ext}}$, thus utilizing the physical contact of the HILS system which is then inserted into the VMS dynamics (15), giving the total manipulator end-effector control force as,

$$F_e = \mu_e \dot{x}_e + \mu_{en} v_n + \left(\Lambda \hat{\Lambda}_e^{-1} - I\right) F_{\text{ext}} \\ + \Lambda \hat{\Lambda}_e^{-1}\left(\hat{F}_e - \hat{\mu}_e \dot{\hat{x}}_e - \hat{\mu}_{en}\hat{v}_n - \hat{\rho}_e\right). \quad (17)$$

As our main goal is controlling the fixed-base system using impedance-matching of the end-effector, the nullspace control law is less vital. We propose a simple nullspace damping approach as follows,

$$F_n = \mu_{ne}\dot{x}_e - D_n v_n, \quad (18)$$

where $D_n = D_n^T > 0$ is a damping gain matrix to be chosen. The nullspace controller cancels out the Coriolis

terms related to the end-effector $\boldsymbol{\mu}_{ne}$, while preserving the nullspace Coriolis $\boldsymbol{\mu}_n \boldsymbol{v}_n$, in order to compensate the effects of the VMS end-effector motion on the manipulator nullspace dynamics. Note that our impedance matching approach is not affected by the damping controller designed for the nullspace dynamics. The impedance matching strategy ensures that the dynamics of the FBM matches that of the VMS end-effector dynamics, and therefore we do not have to separately simulate the end-effector dynamics of the VMS (15). However, the nullspace dynamics of the VMS (16) are simulated to obtain its nullspace velocity $\hat{\boldsymbol{v}}_n$. The inverse Jacobian is then used to reconstruct the joint and base velocities of the VMS as follows,

$$ \hat{\boldsymbol{\nu}} = \hat{\boldsymbol{J}}^{-1} \begin{bmatrix} \dot{\hat{\boldsymbol{x}}}_e^T & \hat{\boldsymbol{v}}_n^T \end{bmatrix}^{\boldsymbol{T}}. \tag{19} $$

These velocities could then be integrated to obtain the joint and base positions $\hat{\boldsymbol{\eta}}$. The numerical integration will however inherently lead to drift. Therefore, instead of using the measurements of the manipulator end-effector velocities directly, we propose a drift compensation strategy as follows,

$$ \dot{\hat{\boldsymbol{x}}}_e = \dot{\boldsymbol{x}}_e + \boldsymbol{K_{dr}} \left((\hat{\boldsymbol{x}}_e - \hat{\boldsymbol{x}}_{e0}) - (\boldsymbol{x}_e - \boldsymbol{x}_{e0}) \right), \tag{20} $$

where $\hat{\boldsymbol{x}}_{e0}$ and $\boldsymbol{x}_{e0}$ are the initial end-effector position of the VMS and FBM, respectively, and $\boldsymbol{K_{dr}}$ is the drift coefficient. Eq. (20) will ensure that the velocity and the position of the VMS end-effector will maintain its fixed initial offset with respect to the corresponding FBM variables, and thus compensate for the drift resulting from numerical integration.

IV. CONTROL APPROACH FOR THE VMS

The proposed HILS scheme is independent of the VMS controller, and therefore any control approach can be chosen for the VMS. The controller may be designed either in the joint space (10), or in the end-effector and nullspace coordinates (12). For a joint-space controller, the control input needs to be transformed into decoupled end-effector and nullspace forces using the following relation,

$$ \begin{bmatrix} \hat{\boldsymbol{F}}_e^{\boldsymbol{T}} & \hat{\boldsymbol{F}}_n^{\boldsymbol{T}} \end{bmatrix}^{\boldsymbol{T}} = \begin{bmatrix} \hat{\boldsymbol{J}}_e^{\boldsymbol{T}} & \hat{\boldsymbol{N}}^{\boldsymbol{T}} \end{bmatrix}^{-1} \hat{\boldsymbol{\tau}}. \tag{21} $$

However, in this study, we designed a decoupled control input for the end-effector and the nullspace dynamics. We choose a PD+ control approach [23] for the end-effector as this is one of the most well-established control approaches. Specifically, the VMS end-effector control input is chosen as

$$ \begin{aligned} \hat{\boldsymbol{F}}_e = & \hat{\boldsymbol{\Lambda}}_e \ddot{\hat{\boldsymbol{x}}}_{e,d} + \hat{\boldsymbol{\mu}}_e \dot{\hat{\boldsymbol{x}}}_{e,d} + \hat{\boldsymbol{\mu}}_{en} \hat{\boldsymbol{v}}_n + \hat{\boldsymbol{\rho}}_e + \\ & \boldsymbol{K_D} \left(\dot{\hat{\boldsymbol{x}}}_{e,d} - \dot{\hat{\boldsymbol{x}}}_e \right) + \boldsymbol{K_P} \left(\hat{\boldsymbol{x}}_{e,d} - \hat{\boldsymbol{x}}_e \right), \end{aligned} \tag{22} $$

where the desired end-effector velocity and position are denoted by $\dot{\hat{\boldsymbol{x}}}_{e,d}$ and $\hat{\boldsymbol{x}}_{e,d}$ respectively. The nullspace controller for the VMS is chosen similar to (18) as,

$$ \hat{\boldsymbol{F}}_n = \hat{\boldsymbol{\mu}}_{ne} \dot{\hat{\boldsymbol{x}}}_e - \hat{\boldsymbol{D}}_n \hat{\boldsymbol{v}}_n + \hat{\boldsymbol{\rho}}_n. \tag{23} $$
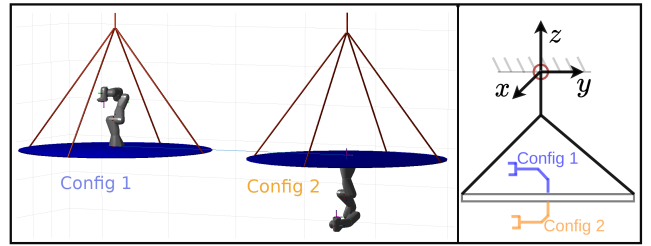

Fig. 2: Two different configurations of the simulated VMS, which consists of a 3-DoF base and a 7-DoF robotic arm. Configuration 1 (on the left) has the robotic arm mounted in an upright position, while configuration 2 (on the right) has the arm mounted in an inverted position. The VMS is suspended using stiff ropes from a crane. The three axes of rotation of the base are also shown in the figure.

V. EXPERIMENTAL VALIDATION

In order to validate our proposed approach for the hardware-in-the-loop simulations, the Franka Research 3 manipulator [17] is used, which consists of seven torque-controlled rotational joints. The end-effector of the Franka robot is fitted with a pointed tip for physical interaction tasks. The Franka was interfaced using the Simulink interface [17] provided by the manufacturer, running at 1000 Hz. The VMS considered for this study is similar to the SAM platform [24], which consists of a fully-actuated suspended base with six degrees of freedom, and a seven degrees of freedom KUKA robotic arm attached underneath it.

The simulated VMS system (Fig. 2) consists of a movable base that is suspended from a crane using a stiff rope of length 3 m. The base consists of three actuation units, which are the rotation of the rope about its hanging point, along the x-, y- and z-axis of the inertial frame. Three joint angles of the VMS-base are used to express the rotation about the three different axes. This gives a total of 10 DoF, so that the entire system state can be described by $\hat{\boldsymbol{q}} \in \mathbb{R}^{10}$, where $\hat{q}_1, \hat{q}_2$ and $\hat{q}_3$ describe the base rotation around the x-, y-, and z-axis respectively. The base of the VMS is assumed to be a rigid disk of mass 10 kg with a Franka manipulator attached to it. We validated our approach using two different configurations of the VMS, which are the upright and the inverted mounting of the manipulator to the base of the VMS. The initial joint angles for the FBM are chosen as 0, $-\pi/4$, 0, $-3\pi/4$, $-\pi/2$, $\pi/2$ and 0 radians, which correspond to the end-effector pointing vertically downwards, which is necessary for the physical interaction task in our work. The manipulator of the VMS has the same initial configuration as the FBM, whereas its base is placed perpendicular to the z-axis of the global frame by commanding its three joint angles as 0 radians. The stiffness and damping gains of the VMS controller are chosen based on their initial VMS end-effector inertia, and are summarized in Table I. For the sake of simplicity, the nullspace gains are chosen as the identity matrix. The proportional components in our controller corresponding to the orientation errors are calculated using relative Euler

angles instead of absolute Euler angles, in order to mitigate singularity issues [25].

Besides this, the external contact forces experienced by the FBM end-effector are calculated using an internal nonlinear disturbance observer [17], rather than using an external force-torque sensor. A second-order low-pass filter with a cut-off frequency of 10 Hz is used to attenuate the noise from the estimator.

TABLE I: Controller Coefficients

	x	y	z	ϕ	θ	ψ
K_P	500	206	278	21.5	61.5	73.5
K_D	30.3	20.1	23.3	6.5	11	12

The experimental validation is accomplished using three different scenarios. In the first scenario, a trajectory tracking task is given to the end-effector of the VMS, and then in the second scenaio, the end-effector is commanded to maintain a fixed position provided as its setpoint, in the presence of external disturbances. Finally in the third scenario, we consider physical interaction, where the end-effector interacts compliantly with the environment, and the corresponding effects in the VMS are analyzed. For the first scenario, both configurations of the VMS are tested, while only configuration 1 is shown for the second and third scenarios, as the performance was found to be similar for both configurations.

A. Trajectory Tracking

For the trajectory tracking task, a sinusoidal signal of amplitude 0.15 m and a frequency of 0.6 rad/s is provided as the reference for the x- and z-axis position, represented in the global coordinate frame. The end-effector position along the y-axis and its orientation are commanded to remain in their initial configurations. The results of the tracking task for the x-axis and z-axis are shown in Fig. 3a for configuration 1 of the VMS, and in Fig. 3b for configuration 2. These plots

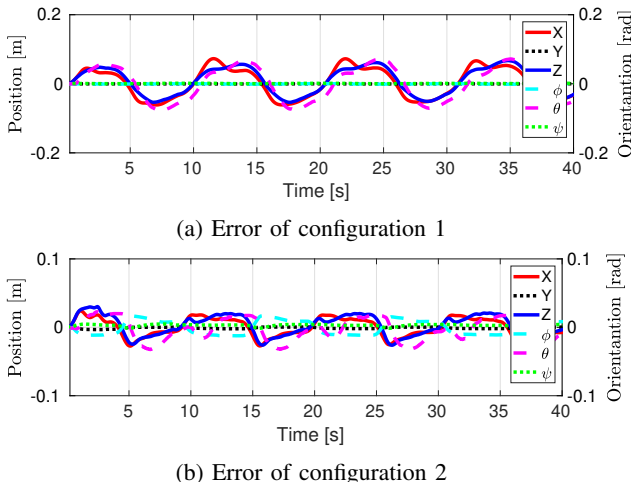(a) Error of configuration 1

(b) Error of configuration 2

Fig. 3: Errors between the reference $\hat{x}_{e,d}$ and the end-effector pose $\hat{x}_e$ of the two configurations of the VMS, for the trajectory tracking task.

show that the PD+ controller in (22) allows the VMS end-effector to successfully track the given reference trajectory, with a tracking error of less than 0.1 m for the position and 0.1 rad for the orientation (Fig. 3). A possible source of this error is the use of a force estimator at the end-effector instead of a physical sensor, due to which the bias and noises from the estimator gets reflected in the control signals. These errors can be reduced by an effective tuning or potentially be eliminated by the use of integral action in the controller, which is not addressed in this paper. We also observe that the rotational error about the y-axis (θ) is similar to that of the translational x- and z- axis errors, due to the coupling of these axes in the end-effector dynamics.

The nullspace velocities corresponding to the redundant DoF are plotted in Fig. 4. The fixed-base robot has one extra DoF, and thus only one nullspace velocity whereas the VMS has four degrees of redundancy. We observe that the nullspace velocities of the VMS oscillates with a frequency matching the reference signal. However, the variation in the redundant DoF does not affect the end-effector dynamics due to the appropriate selection of the nullspace operator N in (4).
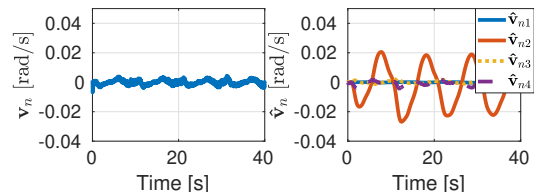

Fig. 4: Nullspace velocities of the FBM (left) and the VMS in configuration 1(right) during the trajectory tracking task.

B. Setpoint Regulation with External Disturbances

In the second scenario, the VMS end-effector was commanded to maintain its initial position and orientation, in the presence of external disturbances (Fig. 5). The external disturbances are applied from around five seconds onwards by a human. These disturbances were applied at the end-effector of the FBM with magnitudes up to around 25 N. From Fig. 5, we can see that the commanded forces of the VMS end-effector were in the opposite direction of the external forces, in order to counteract them. We can also observe that the end-effector forces commanded by the VMS and the FBM are of different magnitudes. The end-effector positions during the setpoint regulation task are plotted in Fig. 6, which depicts that they are compliant with the external disturbances.

C. Physical Interaction

The final scenario is a physical interaction task consisting of four different stages as shown in Fig. 7, in order to demonstrate compliant behaviour of the designed control system on a fixed known environment. In this task, the VMS end-effector is given a reference in the z-direction such that it is able to push against the external object for a few seconds.
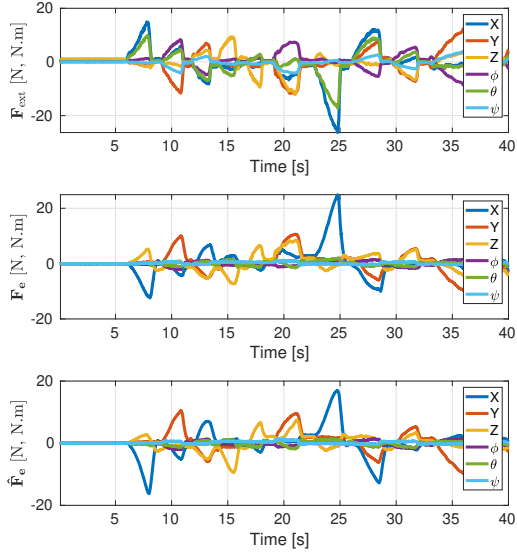
Fig. 5: External disturbances and the corresponding end-effector commanded forces on the FBM and VMS during the setpoint regulation task.
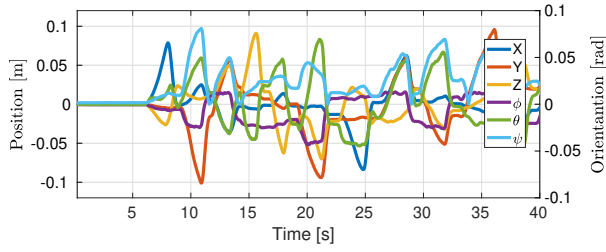

Fig. 6: Deviation of the end-effector pose $\hat{x}_e$ of the VMS from its initial pose $\hat{x}_{e0}$ during the setpoint regulation task, corresponding to the forces shown in Fig. 5

.

The external contact forces during the interaction were taken into account for the impedance matching of the VMS with the FBM. Fig. 8 shows the external forces at the FBM end-effector during the task, with the contact periods highlighted in orange. The contact forces mostly acted along the z-axis of the end-effector, as it was commanded a vertical downward motion during the task. There was however also some effect in the other coordinates, mainly the x and θ coordinates, due to the coupling effect along these axes. The effects of the motion of the end-effector and the external forces experienced by it were reflected in the base-motion of the VMS, which tilts during the task. This can be directly correlated to (12), which describes how the external contact forces F_{ext} affect the end-effector of the VMS, which is related to its base coordinates using (19). In our case, the base of the VMS and the robot moves in the same direction as the base is fully actuated. For a free-floating base, a different motion might be observed which will be investigated in the future work.
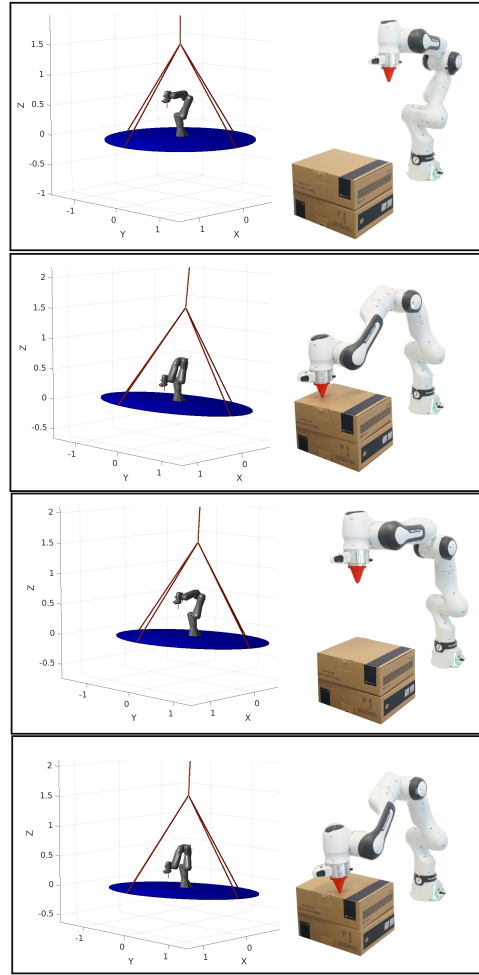

Fig. 7: The VMS and the corresponding configurations of the FBM during the task of physical interaction with the environment. The contact happens with the external object, which is a cardboard box.
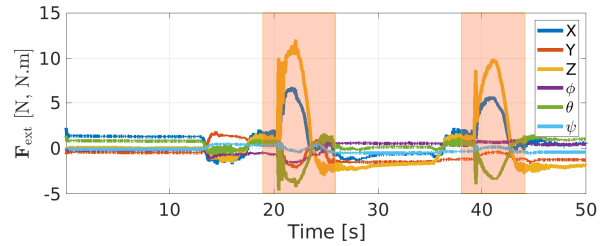

Fig. 8: Contact forces on the end-effector of the FBM during the physical interaction task. The periods of external contact are highlighted using orange markers.

VI. CONCLUSIONS AND FUTURE WORK

In this paper, a novel approach for performing hardware-in-the-loop simulations has been presented, which takes into account the actual contact dynamics of the end-effector with the environment. Our approach is based on an impedance-matching strategy of the end-effector dynamics, while simulating the redundant degrees of freedom of the VMS using

nullspace coordinates. Our approach also compensates for drift in the end-effector position, which can happen due to the numeric integration of the nullspace and end-effector velocities to obtain a full configuration of the VMS. The main benefit of our proposed approach is its generic structure that can be applied to match the end-effector dynamics of a given VMS with a FBM. In this paper, we successfully validated our HILS approach on a 10-DoF suspended aerial manipulator system using the Franka Research 3 robot.

In our future research, we intend to integrate a force-torque sensor to the end-effector of the emulator system instead of relying on estimates of the external forces, which can potentially improve the tracking results. In the future, we also intend to scale the motion of the emulated system, so that a larger or smaller workspace of the VMS can be matched with the given system. Moreover, our HILS approach will be compared with an actual mobile-based-manipulator robot in a lab environment to perform physical interaction tasks.Additionally, we plan to apply our approach to other VMS with more complex dynamics, such as the Eelume autonomous underwater vehicle [26].

ACKNOWLEDGMENT

REFERENCES

[1] H. Mishra, A. M. Giordano, M. De Stefano, R. Lampariello, and C. Ott, "Inertia-Decoupled Equations for Hardware-in-the-Loop Simulation of an Orbital Robot with External Forces," in *Proc. 2020 IEEE/RSJ International Conference on Intelligent Robots and Systems*. Las Vegas, NV, USA: IEEE, Oct. 2020, pp. 1879–1886.

[2] G. Antonelli, *Underwater Robots*, 4th ed. Springer Int. Publishing AG Cham, 2018.

[3] A. Flores-Abad, O. Ma, K. Pham, and S. Ulrich, "A review of space robotics technologies for on-orbit servicing," *Progress in Aerospace Sciences*, pp. 1–26, July 2014.

[4] E. Simetti, "Autonomous Underwater Intervention," *Current Robotics Reports*, pp. 117–122, Sept. 2020.

[5] L. Skrinjar, J. Slavič, and M. Boltežar, "A review of continuous contact-force models in multibody dynamics," *International Journal of Mechanical Sciences*, pp. 171–187, Sept. 2018.

[6] M. Bacic, "On hardware-in-the-loop simulation," in *Proc. 44th IEEE Conference on Decision and Control*, Dec. 2005, pp. 3194–3198.

[7] J. Kiesbye, D. Messmann, M. Preisinger, G. Reina, D. Nagy, F. Schummer, M. Mostad, T. Kale, and M. Langer, "Hardware-in-the-loop and software-in-the-loop testing of the move-ii cubesat," *Aerospace*, 2019.

[8] D. Jung and P. Tsiotras, "Modeling and hardware-in-the-loop simulation for a small unmanned aerial vehicle," in *AIAA Infotech@ Aerospace 2007 Conference and Exhibit*, 2007, p. 2768.

[9] H. K. Fathy, Z. S. Filipi, J. Hagena, and J. L. Stein, "Review of hardware-in-the-loop simulation and its prospects in the automotive area," in *Proc. Modeling and Simulation for Military Applications*. SPIE, May 2006, pp. 117–136.

[10] J.-C. Piedboeuf, J. de Carufel, F. Aghili, and E. Dupuis, "Task verification facility for the Canadian special purpose dextrous manipulator," in *Proc. 1999 IEEE International Conference on Robotics and Automation (Cat. No.99CH36288C)*, May 1999, pp. 1077–1083.

[11] J. Artigas, M. De Stefano, W. Rackl, R. Lampariello, B. Brunner, W. Bertleff, R. Burger, O. Porges, A. Giordano, C. Borst, and A. Albu-Schaeffer, "The OOS-SIM: An on-ground simulation facility for on-orbit servicing robotic operations," in *2015 IEEE International Conference on Robotics and Automation*, May 2015, pp. 2854–2860.

[12] F. Mou, X. Xiao, T. Zhang, Q. Liu, D. Li, C. Hu, and W. Ma, "A HIL Simulation Facility for Task Verification of the Chinese Space Station Manipulator," in *Proc. 2018 IEEE International Conference on Mechatronics and Automation*, Aug. 2018, pp. 2138–2144.

[13] R. Krenn and B. Schaefer, "Limitations of hardware-in-the-loop simulations of space robotics dynamics using industrial robots," *European Space Agency-Publications-ESA SP*, vol. 440, pp. 681–686, 1999.

[14] K. Cetin, H. Tugal, Y. Petillot, M. Dunnigan, L. Newbrook, and M. S. Erden, "A robotic experimental setup with a stewart platform to emulate underwater vehicle-manipulator systems," *Sensors*, vol. 22, no. 15, p. 5827, 2022.

[15] F. Aghili and J.-C. Piedboeuf, "Contact dynamics emulation for hardware-in-loop simulation of robots interacting with environment," in *Proc. IEEE International Conference on Robotics and Automation*, May 2002, pp. 523–529.

[16] E. Cuniato, J. Cacace, M. Selvaggio, F. Ruggiero, and V. Lippiello, "A hardware-in-the-loop simulator for physical human-aerial manipulator cooperation," in *2021 20th International Conference on Advanced Robotics*. IEEE, 2021, pp. 830–835.

[17] S. Haddadin, S. Parusel, L. Johannsmeier, S. Golz, S. Gabl, F. Walch, M. Sabaghian, C. Jähne, L. Hausperger, and S. Haddadin, "The Franka Emika Robot: A Reference Platform for Robotics Research and Education," *IEEE Robotics & Automation Magazine*, pp. 46–64, June 2022.

[18] J. Park, W. Chung, and Y. Youm, "On dynamical decoupling of kinematically redundant manipulators," in *Proc. IEEE/RSJ International Conference on Intelligent Robots and Systems. Human and Environment Friendly Robots with High Intelligence and Emotional Quotients*, Oct. 1999, pp. 1495–1500.

[19] F. Aghili and J.-C. Piedboeuf, "Hardware-in-loop simulation of robots interacting with environment via algebraic differential equation," in *Proc. 2000 IEEE/RSJ International Conference on Intelligent Robots and Systems*, Oct. 2000, pp. 1590–1596.

[20] R. M. Murray, Z. Li, and S. S. Sastry, *A Mathematical Introduction to Robotic Manipulation*, 1st ed. CRC Press, 1994.

[21] Y.-C. Chen and I. D. Walker, "A consistent null-space based approach to inverse kinematics of redundant robots," in *Proc. IEEE International Conference on Robotics and Automation*, 1993, pp. 374–381.

[22] G. Garofalo, B. Henze, J. Englsberger, and C. Ott, "On the inertially decoupled structure of the floating base robot dynamics," in *Proc. 8th Vienna International Conf. on Mathematical Modelling*, 2015, pp. 322–327.

[23] B. Paden and R. Panja, "Globally asymptotically stable 'PD+' controller for robot manipulators," *International Journal of Control*, pp. 1697–1712, June 1988.

[24] Y. S. Sarkisov, M. J. Kim, D. Bicego, D. Tsetserukou, C. Ott, A. Franchi, and K. Kondak, "Development of SAM: Cable-Suspended Aerial Manipulator," in *Proc. International Conference on Robotics and Automation*, May 2019, pp. 5323–5329.

[25] F. Caccavale, C. Natale, B. Siciliano, and L. Villani, "Six-dof impedance control based on angle/axis representations," *IEEE Trans. Robotics and Automation*, pp. 289–300, 1999.

[26] P. Liljebäck and R. Mills, "Eelume: A flexible and subsea resident imr vehicle," in *OCEANS 2017 - Aberdeen*, 2017, pp. 1–4.